Exploring magnetism of lead-free halide double perovskites: A high-throughput first-principles study

Utkarsh Singh ⓘ,[1,*] Johan Klarbring,[1] Igor A. Abrikosov ⓘ,[1] and Sergei I. Simak ⓘ[1,2]

[1]*Theoretical Physics Division, Department of Physics, Chemistry and Biology (IFM), Linköping University, SE-581 83 Linköping, Sweden*
[2]*Department of Physics and Astronomy, Uppsala University, SE-75120 Uppsala, Sweden*

We have performed a comprehensive, first-principles high-throughput study of the magnetic properties of halide double perovskites, $Cs_2BB'Cl_6$, with magnetic ions occupying one or both B and B′ sites. Our findings indicate a general tendency for these materials to exhibit antiferromagnetic ordering with low Néel temperatures. At the same time, we reveal a few potential candidates that predicted to be ferromagnetic with relatively high Curie temperatures. Achieving ferromagnetic coupling might be feasible via simultaneously alloying at B and B′ sites with magnetic 3d and nonmagnetic 5d ions. With this approach, we discover that $Cs_2HgCrCl_6$, $Cs_2AgNiCl_6$, and $Cs_2AuNiCl_6$ have high Curie temperatures relative to their peers, with the latter two exhibiting half metallic behavior. Further, this study illuminates the underpinning mechanism of magnetic exchange interactions in halide double perovskites, enabling a deeper understanding of their magnetic behavior. Our findings, especially the discovery of the compounds with robust half metallic properties and high Curie temperatures, hold promise for potential applications in the field of spintronics.

I. INTRODUCTION

Over the past decade, research on metal halide perovskites has experienced a consistent growth, establishing itself as one of the most dynamic fields within materials science [1]. While the investigation was initially focused on materials containing lead, several lead-free variations have emerged as intriguing alternatives [2]. These subsets primarily aim to overcome the limitations associated not only with the toxicity of lead but also with the poor thermodynamic stability. One particular group of materials that has surfaced as an alternative in recent years is lead-free halide double perovskites (HDPs), wherein the Pb^{+2} ions are substituted with a combination of monovalent and trivalent cations [3].

Lead-free halide double perovskites (LFHDPs) $A_2BB'X_6$ are composed of A ∈ {Cs, Rb}, B ∈ {+1 elements}, B′ ∈ {+3 elements}, and X ∈ {Cl, Br, I}. They present nontoxic and stable alternatives to typical lead-based ABX_3 perovskites with A ∈ {MA⁺, FA⁺, Cs}, B = 2+ toxic element Pb, and X ∈ {F, Cl, Br, I}. Here MA stands for methylammonium and FA stands for formamidinium.

The combination of (+1, +3) ions on (B, B′) sublattices in LFHDPs provides a larger chemical space in comparison to typical $APbX_3$ perovskites, making halide double perovskites,

potentially, a class of multifunctional materials [4,5] similar to Heusler compounds [6] and their oxide counterparts [7]. One facet of this is applications based on their magnetic properties, which require substitution of either or both B and B′ sites with elements having unpaired d electrons.

Recently, several studies have shown that Fe^{+3} can be incorporated in the double perovskite structure in the B′ sublattice when the B sublattice is populated with s-block element Na [8,9] and d-block element Ag [10]. However, unlike their oxide counterparts, for LFHDPs, this has mainly been explored in the context of improving the performance of optoelectronic devices [11,12], leaving out many possible combinations of elements which can populate the structure. We therefore find it important to examine, qualitatively and quantitatively, the nature of magnetic interactions in halide double perovskites.

The double perovskite structure, shown in Fig. 1(a), can be described as two interpenetrating face-centered-cubic (fcc) B and B′ sublattices, with the species A occupying a simple cubic lattice. This structure prohibits the possibility for direct interactions between the magnetic species. This is illustrated in Fig. 1(b) for the case when the latter occupies the B′ sublattice. The dominant exchange path is B′-X-B-X-B′, which has previously been described as a super-superexchange type of magnetic interaction [13,14]. Naturally, the choice of the (B, B′) pair is paramount to enabling the existence of any significant magnetic interactions in this structure.

In this work, we search for the possibility of obtaining magnetic LFHDPs with reasonably high magnetic transition temperatures. We start by examining magnetic exchange parameters (J_i) in typical LFHDPs, where the species occupying the B sublattice are known to have a +1 oxidation state (Ag, Na), while the other are from the 3d series of elements such
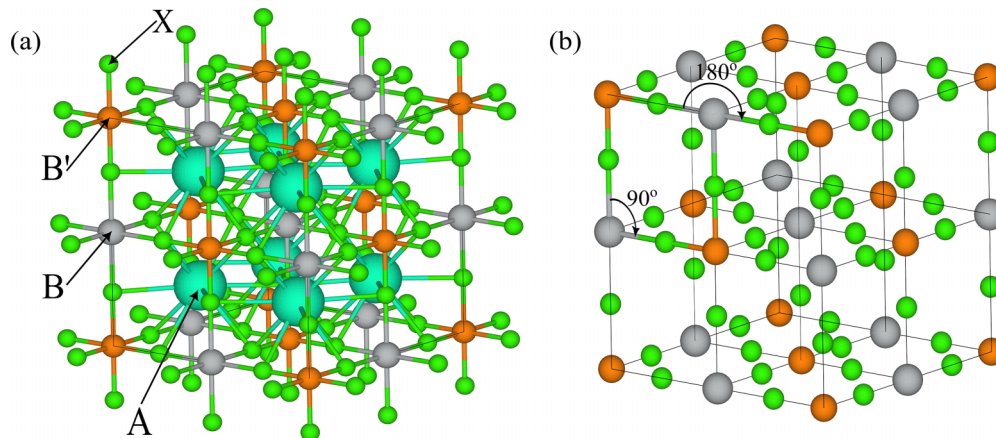
---

*utkarsh.singh@liu.se

FIG. 1. Illustration of (a) conventional unit cell for halide double perovskite structure, $A_2BB'X_6$, A = Cs, Rb, B, B' ∈ +1, +3 or +2, +2 elements, and X = Cl, Br, I, and (b) exchange interaction path, B'-X-B-X-B', where ∠X-B-X = 90° or 180° for first and second coordination shells, respectively.

as Fe and Ni. Then we look at the compounds where B is a nonmagnetic element known to exhibit a +2 oxidation state, while B' is from the 3d series of elements. Finally, we study candidate structures where both B and B' sublattices are populated by $3d^{1-9}$ elements.

II. METHOD

A. Candidate compounds

Since the possible magnetic structures span a large chemical space, we proceed with a high-throughput approach to describe the magnetic properties of lead-free halide double perovskites.

As the first step, we refer to high-throughput databases [15,16] and previous high-throughput studies [17,18] into the structural and thermodynamic stability of LFHDPs and extract 64 candidate compounds (Table S1 [19]) that were predicted to be thermodynamically stable and have one or both B and B' sites populated with a 3d element. We have considered the modified tolerance factor, τ, introduced by Bartel *et al.* [20] as the marker for structural stability of halide double perovskites. For this study, we consider compounds that lie up to 50 meV/atom above the convex hull to account for potential errors due to insufficient cutoff energies, suboptimal k-point sampling, and intrinsic exchange-correlation functional inaccuracies during the generation of these hulls on material databases.

It is prudent to note that during the high-throughput studies, only ferromagnetic structures were considered. As we will demonstrate below, many of the compounds in question depart from their ferromagnetic, cubic perovskite structure and assume a lower symmetry structure in an antiferromagnetic, ferromagnetic, or ferrimagnetic configuration (Table S1 [19]). Naturally, taking these effects into account would affect the stability predictions.

For each of the candidate compounds, we attempt to find their ground state structure within collinear configurations and calculate relevant magnetic exchange interactions. This is followed up by calculating the magnetic transition temperatures via classical Monte Carlo simulations.

B. Magnetic configurations

For compounds with a single magnetic element occupying either the B or B' site, we consider the typical collinear magnetic configurations allowed in the fcc lattice illustrated in Fig. 2(a). For the cases where both B and B' sublattices are occupied by a $3d^1 - 3d^9$ element, we consider the magnetic configurations illustrated in Fig. 2(b).

Certainly, it is possible that some of these structures may assume more complex collinear or noncollinear magnetic configurations. However, what we wish to illustrate is the difference in the nature of magnetic interactions with respect to the choice of B and B' ions within this large chemical space. This difference, as we see later, is highlighted quite well using the chosen configurations.

C. Magnetic exchange interactions

The classical Heisenberg Hamiltonian is defined as

$$H = -\sum_{\langle ij \rangle} J_{ij} S_i \cdot S_j. \tag{1}$$

Here, J_{ij} represents the exchange interaction between spins at sites i and j and S_i and S_j are the spin vectors at these sites. The sum is over all pairs of spins, i ≠ j, in the system.

We calculate the relevant magnetic exchange interactions following the methodology suggested by Xiang *et al.* [21,22], which is based on the calculation of the total energy of the system with collinear spin alignment when spin states of any two chosen sites, say 1 and 2 within a given unit cell, are modified. Within this method, assuming that the magnetism is fully described by the classical Heisenberg Hamiltonian, Eq. (1), the total energy is

$$E = -n J_{12} S_1 \cdot S_2 - S_1 \cdot h_1 - S_2 \cdot h_2 + E_{all} + E_0. \tag{2}$$

In the first term, n is the number of equivalent bonds with exchange coupling J_{12}, $h_1 = \sum_{i \neq 1,2} J_{1i} S_i$, and $h_2 = \sum_{i \neq 1,2} J_{2i} S_i$. The second term $E_{all} = \sum_{i,j \neq 1,2} J_{ij} S_i \cdot S_j$ and the last term E_0 consists of all nonmagnetic energy contributions.

In order for the values to be comparable to other methods, we set $|S_1| = |S_2| = 1$. Then, the relevant exchange interactions between any sites 1 and 2 in the cell can be expressed
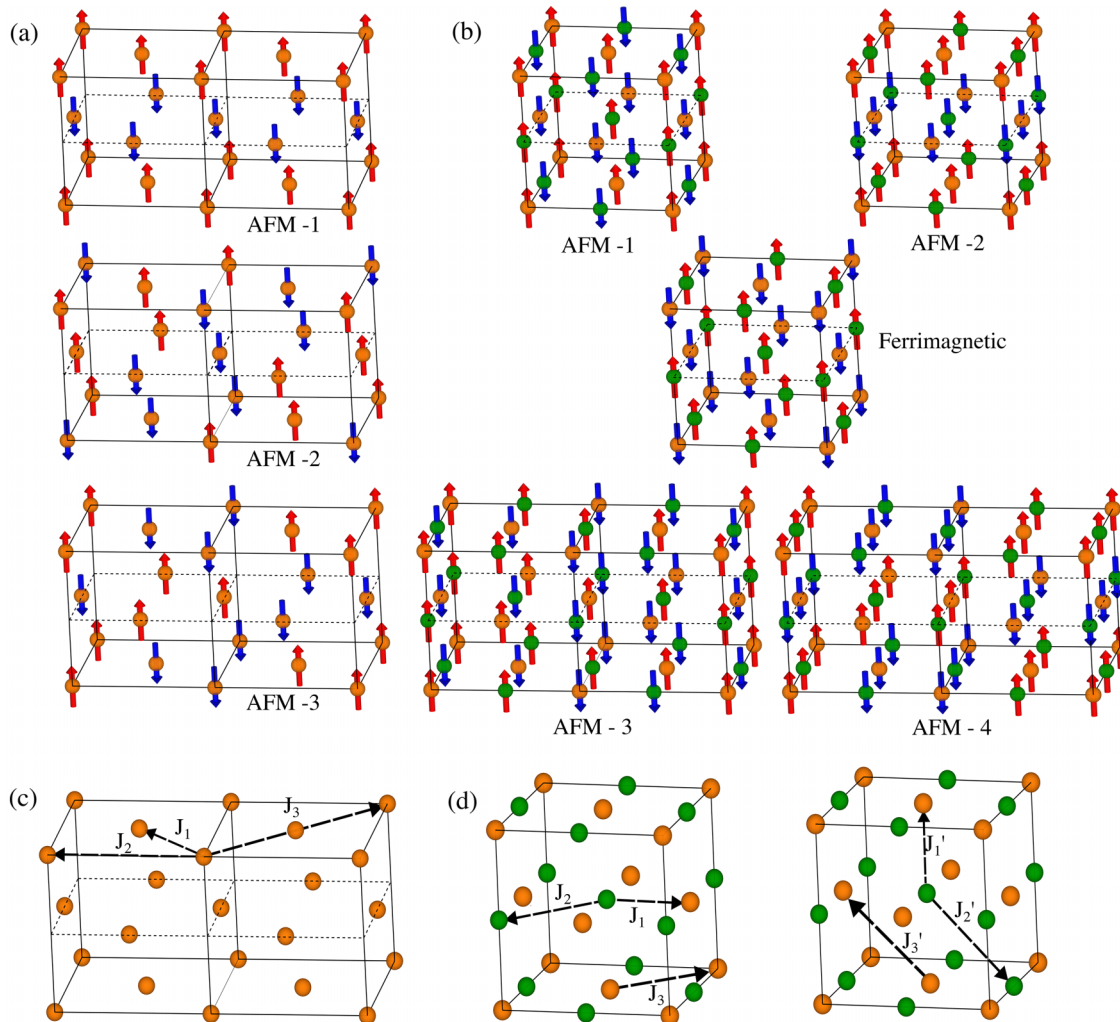
FIG. 2. Magnetic configurations for LFHDPs with (a) B = nonmagnetic ion and B$'$ = magnetic ion and (b) B, B$'$ = magnetic ion. Panels (c) and (d) illustrate the relevant exchange interactions taking tetragonal distortions into account for candidates illustrated in (a) and (b), respectively. The c = 0.5 plane is indicated by dashed lines.

as

$$J_{12} = \frac{E_{\uparrow\downarrow} + E_{\downarrow\uparrow} - E_{\uparrow\uparrow} - E_{\downarrow\downarrow}}{4n}, \qquad (3)$$

where $E_{\uparrow\downarrow}$ corresponds to spin-up on site 1 and spin-down on site 2 and so on.

Specifically, starting from a cubic, 40 atom supercell, we relax the structure in each of the explored magnetic configurations for all candidates. Further, in order to extract the magnetic exchange interactions, we assume the lowest calculated energy state as the reference configuration and use its 160 atom supercell to calculate relevant J_{ij}'s. This procedure provides good convergence of the results.

In the text following this section, we abbreviate the exchange interaction for the nearest-neighbor species 1 and 2 as J_1, the second nearest-neighbor species 1 and 2 as J_2, and so on. Similarly, J_i' refers to the out-of-plane exchange interaction as illustrated in Fig. 2(d).

III. COMPUTATIONAL DETAILS

The density functional theory (DFT) computations were performed with the Vienna *ab initio* simulation package (VASP) [23–25] using the projector augmented-wave (PAW) method [26] with a plane wave cutoff ENCUT set to 1.5 times the maximum ENMAX in the employed PAW potentials. The recommended VASP PAW potentials for each element [27] were used for this study. We performed full structural relaxation with a convergence criterion of 10^{-8} eV for total energy in self-consistent field cycles and <1 meV/Å for atomic forces. A k-point density of 0.15 Å^{-1} for structural relaxations and 0.10 Å^{-1} for accurate total energy calculations was used throughout via the KSPACING tag in VASP.

The PBEsol [28] exchange-correlation functional with Hubbard U correction was used for geometry optimization as well as the calculation of the density of states. We choose the value of the effective on-site correction, U_{eff} [29], to be a uniform value of 3 eV in this study, which has recently been shown to produce results comparable to hybrid functionals when reproducing the electronic and magnetic properties of this class of materials [30].
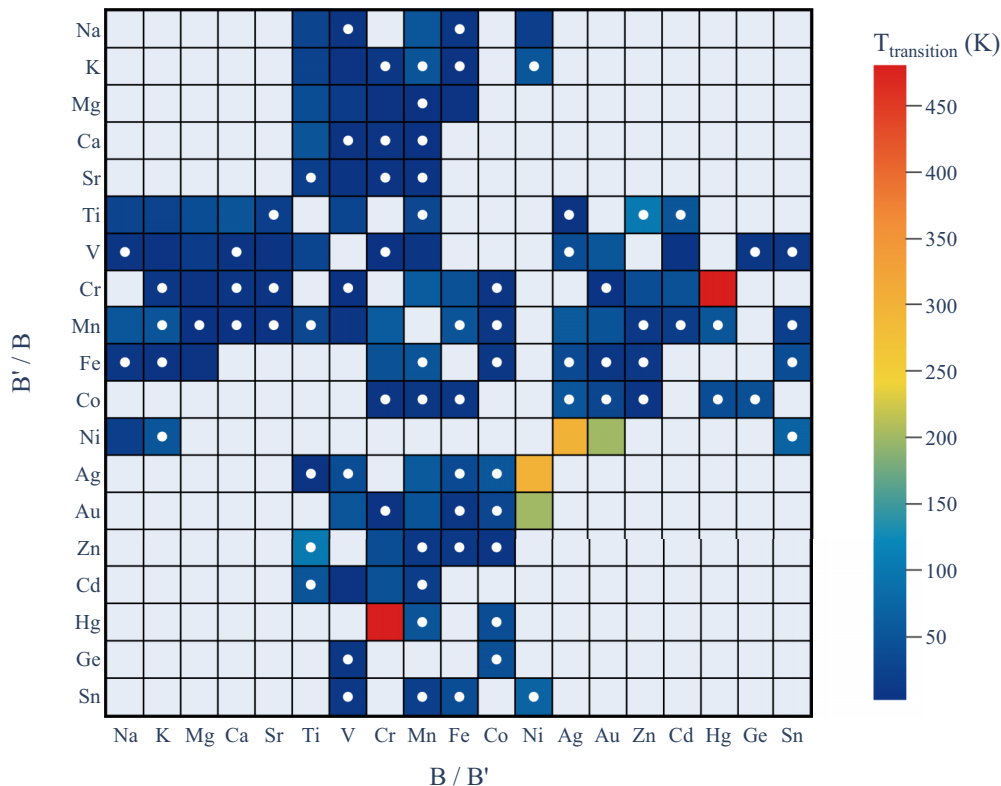
FIG. 3. Magnetic transition temperatures for thermodynamically stable LFHDPs, $Cs_2BB'Cl_6$. The grid squares with white dots represent Néel temperatures, while those without represent Curie temperatures. Empty grid squares indicate structurally or thermodynamically unstable compositions ($E_{hull} > 0.050$ eV/atom). Elements on both axes are grouped by their occurrence among alkali metals, alkaline earth metals, transition metals, triels, and tetrels in the Periodic Table, respectively, and then by increasing atomic numbers within each group.

As we show in Fig. S2 [19], a higher value of U_{eff} might in some cases slightly increase strengths of J_i, therefore leading to a slightly higher value of predicted $T_{transition}$.

The Monte Carlo (MC) simulations were performed with the UPPASD [31] code using the exchange interactions obtained via DFT calculations. Starting from a temperature of 1000 K and moments aligned in a ferromagnetic configuration, a temperature sweep was performed down to 1 K in order to observe the magnetic phase transition by identifying the temperature at which the curves for fourth-order reduced Binder's cumulant U^* [32–34] calculated at different system sizes intersect. Due to low ordering temperatures in many cases, the heat bath Monte Carlo algorithm, as implemented in the UPPASD code, was used to effectively sample the configuration space.

Details on chemical bonding were obtained from a crystal orbital Hamiltonian population (COHP) [35] analysis as implemented in the LOBSTER package [36–38].

The phonon spectra within the harmonic approximation were computed using the PHONOPY [39,40] package. A $2 \times 2 \times 2$ supercell was employed and the interatomic force constants were obtained from DFT calculations. The harmonic approximation was adopted throughout the calculations, which is valid at temperatures near 0 K where anharmonic contributions are negligible. When necessary, the plane wave cutoff was increased to 800 eV to achieve convergence. We find that, in the presence of a rather flat potential energy surface, careful calculations with appropriately large plane wave energy cutoff are needed to obtain the proper, dynamically stable structure.

IV. RESULTS

Figure 3 illustrates the magnetic transition temperatures, as predicted from MC simulations, for the LFHDPs that are the focus of this study. While we predict the majority of the compounds to be magnets with low transition temperatures, this study reveals a few noteworthy exceptions in $Cs_2AgNiCl_6$, $Cs_2AuNiCl_6$, and $Cs_2HgCrCl_6$.

These compounds stand out due to much higher magnetic transition temperatures in comparison to other double perovskites with similar chemistry. In the case of $Cs_2AgNiCl_6$, we find $T_{transition}$ to be $\sim$190 K, while for $Cs_2AuNiCl_6$ it is predicted to be slightly higher at $\sim$240 K. Both of these LFHPs undergo tetragonal distortion (Table II). For $Cs_2HgCrCl_6$, which retains its cubic phase, $T_{transition}$ is predicted to be much higher at $\sim$430 K. We predict all three of these compounds to be ferromagnets. All three of these double perovskites are found to be dynamically stable (Fig. S3 [19]).

Another interesting feature that is observed in the electronic structure of Cs_2BNiCl_6 (B = Ag, Au) is half metallicity [41,42], as illustrated in the insets of Figs. 4(a) and 4(b), respectively. Here, one of the spin channels stays metallic with the other exhibiting insulating behavior. This leads to 100% spin polarization at the Fermi level (E_F). As half metals naturally produce highly

TABLE I. In plane (J_1, J_2, J_3) and out of plane (J_1', J_2', J_3') magnetic exchange parameters, as illustrated in Fig. 2(d). Both B and B′ atoms belong to the 3d series of elements.

B	B′	J_1	J_1'	J_2	J_2'	J_3	J_3'	c/a
Ti	Mn	−7.61		−6.94		−8.4		1.00
	V	−5.84		13.90		−6.80		1.00
V	Cr	−11.17	−10.11	0.03	−0.02	−0.23	−0.12	**1.06**
	Mn	1.32		−0.33		0.06		1.00
Cr	Co	−19.96	−16.99	−0.07	−0.06	0.10	0.08	**1.05**
	Fe	9.72	8.16	0.49	0.36	−0.53	−0.39	**1.03**
	Mn	7.97	6.96	0.66	0.71	−0.25	−0.21	**1.04**
Mn	Co	−10.61		0.72		−1.71		1.01
	Fe	−9.77		−4.92		12.47		0.99
Fe	Co	−7.01	−8.12	0.11	0.12	−0.17	−0.24	**0.97**

spin-polarized currents, they are prime candidates for spintronic devices [43].

We note that, for the case when B, B′ = {Ag, Ni}, where ordered magnetism survives up to $T_c \sim$ 190 K, the calculated gap in the insulating channel is 1.4 eV, which is larger than some known half metallic ternary [44] and quaternary [45] Heusler alloys that have been proposed for use in spintronics. For B, B′ = {Au, Ni}, where the ferromagnetic to paramagnetic transition is expected to be at $T_c \sim$ 240 K, this gap is nearly half of that, at 0.8 eV. A large gap, and more importantly the unavailability of electronic states near the Fermi level in the insulating channel, contributes to the robustness of the half metallic nature [42] towards the influence of defects, impurities, and temperature effects in these compounds.

Having delineated the intriguing feature of half metallicity in these systems and its implications for spintronics, we now turn to the aspect that provides fundamental understanding of their magnetic behavior. A multitude of magnetic properties—including the magnetic transition temperatures, susceptibility, coercivity, remanence, and the critical field for magnetic phase transitions—are primarily determined by the strength and nature of exchange interactions within the material.

In particular, the main focus of this work, the magnetic transition temperatures, are intimately tied to the robustness of exchange interactions, which equates to resisting thermal per-

TABLE II. Comparison of partial (-)ICOHP for B-B′, B-X, B′-X, B-B, and B′ − B′ interactions in representative oxide and halide double perovskite structures. Values are expressed per pairwise interaction. r_1, r_1' = in-plane, out-of-plane B-X bond lengths; r_2, r_2' = in-plane, out-of-plane B′-X bond lengths.

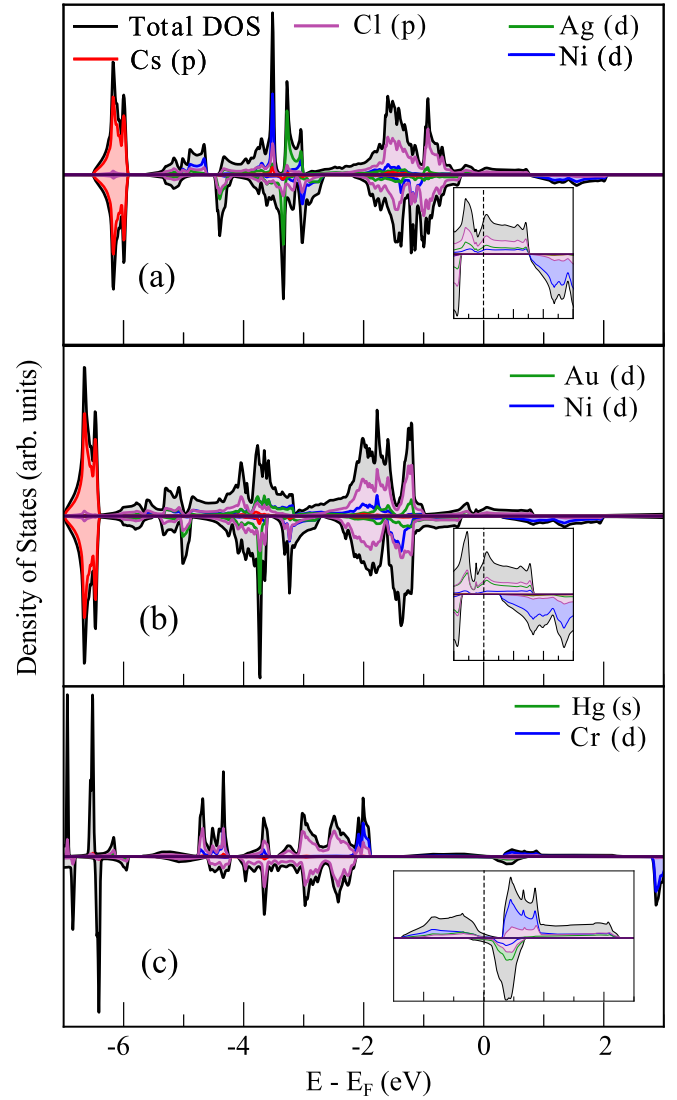| A	B	B′	X	B-B′	B-X	B′-X	r_1, r_1'	r_2, r_2'
Sr	Mo	Fe	O	0.099	1.681	0.718	1.93, 1.93	2.00, 2.00
Sr	Re	Fe	O	0.016	2.332	0.904	1.94, 1.94	1.98, 1.98
Cs	Ag	Fe	Cl	0.010	0.340	0.760	2.68, 2.60	2.39, 2.41
Cs	Au	Fe	Cl	0.014	0.194	0.826	2.87, 2.36	2.35, 2.51
Cs	Ag	Ni	Cl	0.014	0.831	0.735	2.52, 2.76	2.39, 2.28
Cs	Au	Ni	Cl	0.020	0.942	0.580	2.43, 3.11	2.46, 2.21
Cs	Ag	Mn	Cl	0.015	0.466	0.585	2.61, 2.61	2.44, 2.44

FIG. 4. Density of states for $Cs_2BB'Cl_6$, B ∈ {Ag, Au, Hg}, and B′ ∈ {Ni, Cr}. The Fermi level is set to zero.

turbations at higher temperatures and subsequently enhancing the transition temperature. Further, properties like magnetic susceptibility and coercivity are substantially modulated by these interactions.

Therefore, unravelling the intricacies within the mechanism of exchange interactions is paramount to a comprehensive understanding and potential manipulation of the magnetic response in these double perovskite systems. With the following analysis, we aim to shed light on these facets.

Discussing experimentally known alloys $Cs_2NaFeCl_6$ [8,9] and $Cs_2AgFeCl_6$ [10] first, which belong to the B, B′ ∈ (+1, +3) space, we observe that the exchange interactions when B = Ag are an order of magnitude larger than when B = Na (Fig. 5). This is due to the interactions along the path B′-X-B-X-B′ being mediated by a p-d hybridized orbital, like Ag(d)-Cl(p) for the former, as opposed to when there are no p-d interactions and the bonds between the B^+ species and the ligand have mainly ionic character, as in the latter case. In addition, for both types of compounds, the exchange interactions beyond the first shell are quite weak in comparison to J_1.
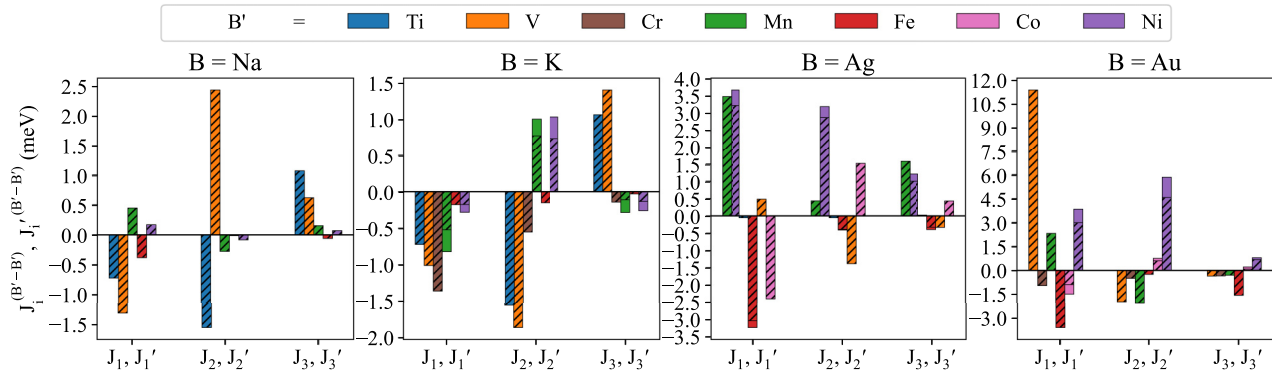
FIG. 5. J_i, J_i' for thermodynamically stable LFHDPs $Cs_2BB'Cl_6$; $B \in$ (Ag, Au, K, Na) and $B' \in 3d^{1-9}$. The dashed bars represent out-of-plane exchange interactions J_i', while the solid bars represent in-plane exchange interactions J_i.

Expectedly, the same trend is observed for their analogs Cs_2KFeCl_6 and $Cs_2AuFeCl_6$.

For the two compounds with standout $T_{transition}$ when B, $B' \in \{+1, +3\}$, $Cs_2AgNiCl_6$ and $Cs_2AuNiCl_6$, the ferromagnetic configuration departs from the cubic perovskite symmetry due to tetragonal distortion and is more stable than the calculated antiferromagnetic configurations which also undergo distortion upon relaxation. We attribute the distortion mainly to Ni^{+3} having a Jahn-Teller (JT) active $3d^7$ configuration as it occurs regardless of how neighboring spins are aligned relative to each other.

In addition, the exchange interactions do not decay as rapidly with the distance between magnetic ions compared to other cases, which is the likely factor that drives up the magnetic transition temperatures.

Apart from these exceptions, we predict all +1, +3 combinations of elements on B, B' to exhibit $T_{transition}$ around or below 50 K as illustrated in Fig. 3. It is also worthwhile to note that for some combinations of B, B' elements, while the strength of magnetic interactions does not decay as quickly with distance, ordering temperatures are still low. This is attributed to the alternation of ferromagnetic and antiferromagnetic interactions with increasing distance. While the presence of ferromagnetic interactions promotes long range order, competing antiferromagnetic interactions introduce magnetic frustration in the system, thus lowering ordering temperatures and resulting in weaker magnets.

Figure 6 shows the calculated values of J_i, J_i' for different LFHDPs, where B $\in$ {Mg, Ca, Sr, Zn, Cd, Hg, Ge, Sn}. Akin to when B, $B' = (+1, +3)$ element, the majority of magnetic exchange interactions, when both B and B' elements are populated by species in +2 oxidation state, are also small and decay rapidly beyond the first coordination shell. This is again, in part, owed to large interatomic distance ≈ 7 Å between nearest-neighbor magnetic ions. For the case of the exception observed when B, $B' = \{Hg, Cr\}$, the exchange interactions across the first three shells are all ferromagnetic and do not decay as quickly with interatomic distance. Interestingly, the ferromagnetic configuration retains the cubic symmetry, while antiferromagnetic configurations undergo significant tetragonal distortion, indicating the effect of spin-lattice coupling.

As shown in Fig. 4(c) (inset), rather unconventional $Cr(t_{2g})$-Hg(s) hybridized states are observed around the Fermi level, pointing to a peculiar picture, where, in addition to the typical B-X interactions mediating the exchange, a direct B'-B interaction might also provide a significant contribution. The calculated ferromagnetic configuration reveals a magnetic moment of $\approx 3.4\mu_B$/atom, indicating that the Cr^{+2} ion is in high spin d^4 configuration.

It is known that d-block elements in the 3d series can exhibit various oxidation states as a function of their chemical environment, which makes it a possibility for LFHDP systems to accommodate two 3d elements on the (B, B') sites. Coupled with the fact that when both B and B' sites are populated with a $3d^{1-9}$ element, the nearest-neighbor distance between two nearest-neighbor magnetic atoms is reduced and this makes for a captivating study where significant magnetic interactions may be expected.

The results of this study are summarized in Table I where we can identify three distinct distributions of exchange interactions. For elemental combinations (V, Cr/Mn), (Cr, Co/Fe/Mn), and (Fe, Co), the nearest-neighbor interactions are an order of magnitude stronger than the second and third nearest-neighbor interactions. For (Ti, Mn/V) and (Mn, Co/Fe), the first, second, and third nearest-neighbor exchange interactions do not decay as quickly and exhibit relatively larger exchange interactions compared to the compounds discussed previously. Unsurprisingly, many of these alloys do deviate from the ideal cubic perovskite structure and end up in a lower symmetry tetragonal structure which is also reflected in the difference between in- and out-of-plane exchange interactions. We highlight significant (c/a > 1.01 or c/a < 0.99) distortions from the ideal perovskite structure in the magnetic ground state. This happens for the following B, B' pairs: (V, Cr), (Cr, Co), (Cr, Fe), (Cr, Mn), and (Fe, Co). The distortions can again be attributed to symmetry breaking via JT-like effects as it is likely that many of these 3d elements exist in JT active d-shell configurations.

Even though these compounds were previously predicted to be thermodynamically stable [18], as summarized in Table S1 [19], we find that, with the exception of (Co, Mn), there are isolated d bands above the main valence band which indicate electronic instability (Fig. S1 [19]) in the structure originating from the fact that one of the d-block species occupying either
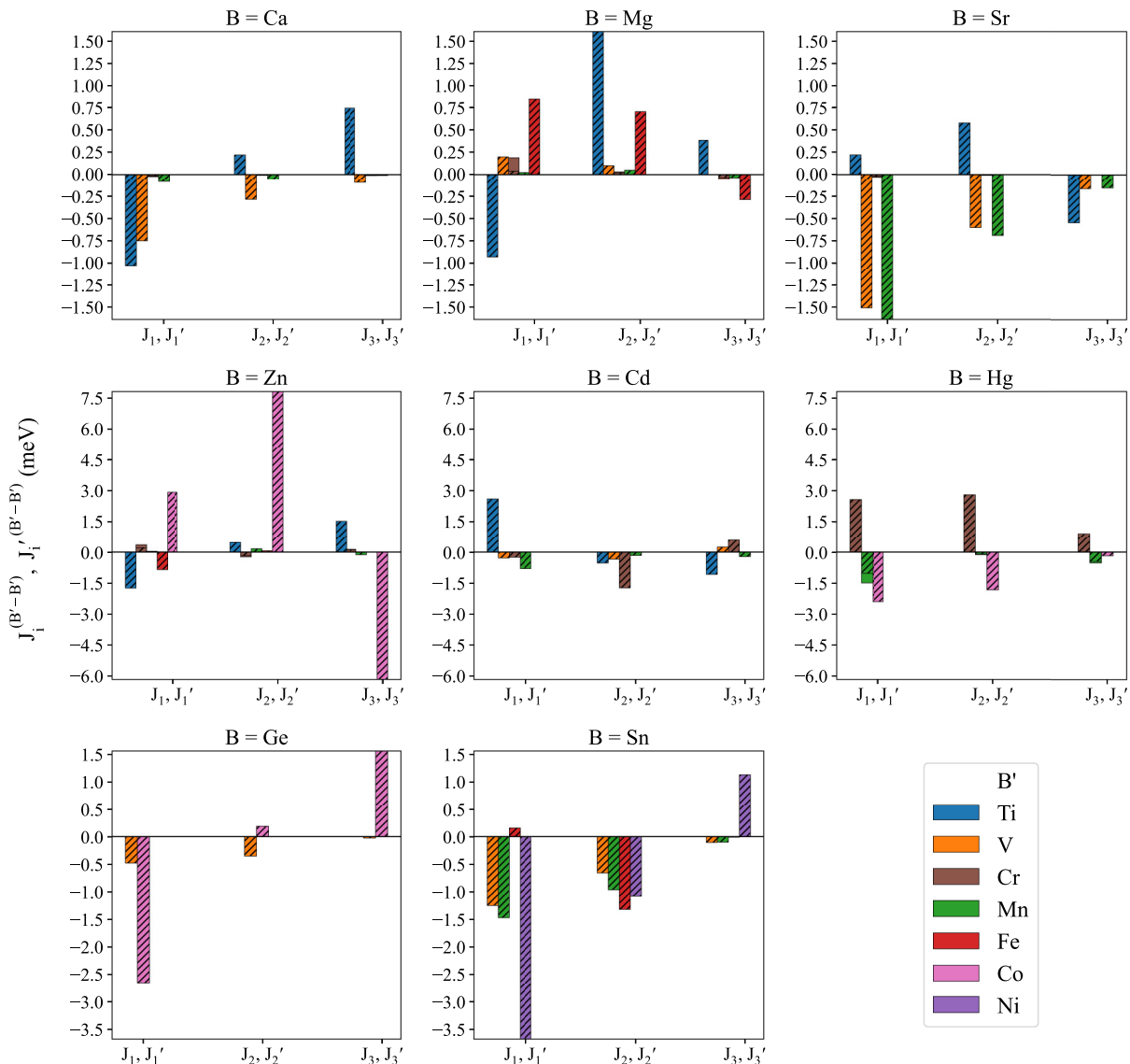
FIG. 6. J_i, J_i' for thermodynamically stable LFHDPs $Cs_2BB'Cl_6$; $B \in \{Mg, Ca, Sr, Zn, Cd, Hg, Ge, Sn\}$ and $B' \in 3d^{1-9}$. The dashed bars represent out-of-plane exchange interactions J_i', while the solid bars represent in-plane exchange interactions J_i.

B or B' sublattices is not in the desired $(+2, +2)$ or $(+1, +3)$ oxidation states.

Similar behavior is also observed for the case of B, $B' \in \{+1\text{ element}, V\}$, where isolated peaks originating from vanadium d bands are present (Fig. S1 [19]), indicating that vanadium might not be in the desired $+3$ oxidation state when $B \in Na, K$. A general trend that we observe is that when the mediating B-X bond has a majority ionic character, such as when $B \in \{Na, K, Ca, Mg, Sr\}$, poor mediation of magnetic exchange via the super-superexchange mechanism (Figs. 5 and 6), and lower magnetic transition temperatures (Fig. 3) as a result, may be expected. Further, while p-d hybridization between the mediating B and X ions is preferred for larger exchange coupling, it is not the sufficient condition for obtaining larger magnetic transition temperatures, owing to another observed trend of alternation between ferromagnetic and antiferromagnetic exchange interactions across different coordination shells. It is possible that such trends might find their origin in the nature of the super-superexchange mechanism that governs the magnetic interactions in these DPs. However, further investigation into the role of mediating and magnetic ions within this mechanism might require delving into the explicit calculation of the contribution of orbital coupling [46] towards the exchange tensor.

It is also worthwhile to note that many vacancy-ordered halide double perovskites have been reported to exist [47–50], making it a possibility for transition metal based perovskites with incompatible oxidation states to adopt similar, perovskite-derived structures. In addition, the transition metal based vacancy-ordered double perovskite Cs_2TiX_6 (X = Cl, Br) [51] was also reported recently, indicating that Ti might prefer to be in a $+4$ oxidation state in the HDP structure. We also do not expect the 3d transition metals at either site to have $+1$ oxidation state as it is not commonly observed.

Recently, a few related structures with reduced dimensionality have been proposed to accommodate elements with oxidation states incompatible with the typical 3D double perovskite structure [52]. While we do not go on to investigate this structural prototype here, we note that it might be possible to have stronger magnetic interactions in such structures and encourage future work to explore this subject.

As illustrated in Fig. 1(b), the dominant path for exchange interaction between the first two nearest neighbors (NN) is B′-X-B-X-B′, where X-B and B-X bonds have a 90° and 180° angle between them for the first and second NN exchange paths, respectively. Naturally, the extent and type of B′-X and B-X interactions in the double perovskite structure affect the strength of this super-superexchange type magnetic interaction.

A comparison between magnetic properties of halide double perovskites (DP) can be made against their analogs in oxide double perovskites ($A_2MM'O_6$) as the exchange paths are presumed to be similar [53]. Here, $A \in +2$ ions (Ca, Sr) and M, M′ are typically metals with oxidation states summing up to +8. We choose a few model compounds in $Sr_2FeM'O_6$ where, like LFHDPs, the A site is populated with an s-block element. Substituting M = Mo, Re produces ferromagnets with $T_c \sim 450$ K [54] and $T_c \sim 600$ K [55], respectively, while M = W shows a low Néel temperature of ~ 37 K [56]. As far as magnetism is concerned, we highlight some key differences between the halide double perovskites considered in this study and the above-mentioned oxide double perovskites.

First, the nearest-neighbor distance between magnetic atoms is shorter in oxide double perovskites, which may enable easier mediation of exchange interactions. This should invariably affect the strength of covalent interactions, which is key to the mediation of exchange interactions. To quantify the extent of covalent bonding between each pair of species, we perform a COHP analysis [30] and calculate the values of -ICOHP, which is the partial -COHP values integrated up to the Fermi level, presented in Table II. While the strength of other interactions is comparable, the mediating B-X interactions are much stronger when X = O compared to when X is a halide. This difference could provide insight into why many oxide perovskites are observed to have high magnetic ordering temperatures, while most halide double perovskites do not, as this study reveals.

Finally, most halide DPs where the B′, B or both sublattices are populated with d-block elements undergo a tetragonal distortion in their predicted, stable ground-state magnetic configuration, which is owed to JT-like distortion, spin-lattice coupling, or a combination of both, as summarized in Table S1 [19]. Large distortions effectively decrease the number of nearest neighbors for each shell, causing a decrease in significant magnetic interactions as well.

V. DISCUSSION

Our findings reveal that HDPs, with either one or both of B, B′ sites occupied with a magnetic ion, predominantly form antiferromagnetic configurations with low Néel temperatures. Despite having a similar super-superexchange type mechanism as oxide double perovskites (ODPs), HDPs do not typically exhibit large magnetic ordering temperatures. We

attribute this phenomenon to factors including comparatively larger interatomic distances, denoted by r_1, r_1' and r_2, r_2' in Table II and weaker interactions between the mediating B and X species in HDPs, which leads to less effective exchange coupling and smaller $T_{transition}$ in turn.

It is possible that octahedral tilting of the $B'X_6$ octahedra could modulate exchange interactions in double perovskites by reducing orbital overlap, which is crucial for magnetic exchange propagation. Unlike ABX_3 type perovskites where a superexchange mechanism, mediated by the "X" anion, is prevalent, magnetism in double perovskites is believed to be facilitated via a super-superexchange mechanism. The effect of octahedral tilting might be less pronounced in double perovskites due to the large interatomic distances (~ 7 Å) between the magnetic ions.

However, we have identified potential half-metallic LFHDPs in $Cs_2AgNiCl_6$, $Cs_2AuNiCl_6$, and $Cs_2HgCrCl_6$ that have not yet been observed experimentally and may exhibit high Curie temperatures. 100% spin polarization at the Fermi level combined with relatively high Curie temperatures might make them attractive candidates towards applications in spintronics [43]. Aside from these select candidates, ferromagnetic configurations are generally not preferred.

Alloying at either one or both B and B′ sites has emerged as a popular strategy for modulating optical properties in HDPs [57–59] and a similar strategy might help drive the nearest-neighbor interactions towards ferromagnetic coupling in order to drive up the magnetic transition temperatures. However, we posit that the effect of sublattice mixing on the strength of magnetic interactions would likely not be significant enough to promote a substantial change in the transition temperatures. And, even in these cases, the Curie temperatures are expected to remain low due to the inherent limitations posed by the structural factors mentioned above.

With the exception of the three candidates mentioned above, in general, this class of compounds may not prove to be promising for magnetic applications beyond 100 K. Some low-temperature magnetic applications, however, may benefit from the usage of nontoxic and low-cost alternatives to typical magnets, such as halide double perovskites.

It has been shown that magnetic materials with low ordering temperatures can exhibit large magnetocaloric effects when alloyed with rare-earth metals [60–64], which can enhance the efficiency of the cooling cycle in magnetic refrigeration systems. Recently, many rare-earth free candidates for magnetic cooling applications have also been reported [65–67]. In addition to this, since materials with low magnetic ordering temperatures allow for faster magnetization switching [68,69], the performance of a novel device such as magnetoresistive random access memory (MRAM) in cryogenic computing could conceivably also benefit from the use of magnetic LFHDPs.

It should be noted that, while this work has explored the available chemical space of transition metal containing LFHDPs obtained via existing studies into their thermodynamic and structural stability, we have not exhausted the entire chemical space of transition metal containing LFHDPs. It is possible that, with a more precise calculation of the convex hull of many other LFHDPs with different species of A, such as Rb^+, and X (= Br, I), additional candidates could be

identified for further exploration of magnetic properties. This approach would involve considering the different magnetic phases for these candidate LFHDPs, as well as those for competing phases. The underlying mechanisms of magnetic interactions revealed through this study should still hold generally true with a different choice of A and X species in the $A_2BB'X_6$ LFHDP structure.

Finally, although halide double perovskites may not be suitable for high-temperature magnetic applications due to the inherent structural factors that lead to lower transition temperatures, they possess potential for low-temperature applications, offering environmentally friendly and cost-effective alternatives to conventional magnetic materials. Future research could focus on the experimental realization of the proposed ferromagnetic candidates and further exploration of alloying strategies for optimizing magnetic properties in halide double perovskites, while taking into account the underlying structural limitations.

VI. CONCLUSIONS

In this study, we have systematically investigated the magnetic properties of halide double perovskites, focusing on the effect of mediating ions on the strength of exchange interactions and resulting magnetic transition temperatures.

The studied LFHDPs show a general propensity towards antiferromagnetic ordering with Néel temperatures less than 50 K. However, some ferromagnetic candidates with relatively high Curie temperatures are discovered.

While $Cs_2HgCrCl_6$ is predicted to have a Curie temperature of 450 K, which is comparable to known oxide double perovskites, $Cs_2AgNiCl_6$ and $Cs_2AuNiCl_6$, with Curie temperatures around 200 K, are predicted to be half metals and proposed for potential use in spintronics. A generally high on-site magnetic moment in the paramagnetic state is also predicted.

By contextualizing the nature of magnetic exchange interactions within the strength and type of bonding interactions, using COHP analysis, we reveal the reasons behind the predicted magnetic properties.

[1] A. K. Jena, A. Kulkarni, and T. Miyasaka, Halide perovskite photovoltaics: Background, status, and future prospects, Chem. Rev. **119**, 3036 (2019).

[2] W. Ning and F. Gao, Structural and functional diversity in lead-free halide perovskite materials, Adv. Mater. **31**, 1900326 (2019).

[3] F. Igbari, Z.-K. Wang, and L.-S. Liao, Progress of lead-free halide double perovskites, Adv. Energy Mater. **9**, 1803150 (2019).

[4] H. Lei, D. Hardy, and F. Gao, Lead-free double perovskite $Cs_2AgBiBr_6$: Fundamentals, applications, and perspectives, Adv. Funct. Mater. **31**, 2105898 (2021).

[5] K. Zhu, Z. Wang, H. Xu, and Z. Fu, Development of multifunctional materials based on heavy concentration Er^{3+} - activated lead-free double perovskite $Cs_2NaBiCl_6$, Adv. Opt. Mater. **10**, 2201182 (2022).

[6] T. Graf, C. Felser, and S. S. Parkin, Simple rules for the understanding of heusler compounds, Prog. Solid State Chem. **39**, 1 (2011).

[7] S. Vasala and M. Karppinen, $A_2B'B''O_6$ perovskites: A review, Prog. Solid State Chem. **43**, 1 (2015).

[8] B. Zhang, J. Klarbring, F. Ji, S. I. Simak, I. A. Abrikosov, F. Gao, G. Y. Rudko, W. M. Chen, and I. A. Buyanova, Lattice dynamics and electron–phonon coupling in double perovskite $Cs_2NaFeCl_6$, J. Phys. Chem. C **127**, 1908 (2023).

[9] M. Armer, P. Dörflinger, A. Weis, C. Büchner, A. Gottscholl, J. Höcker, K. Frank, L. Nusser, M. T. Sirtl, B. Nickel, T. Bein, and V. Dyakonov, Low temperature optical properties of novel lead-free $Cs_2NaFeCl_6$ perovskite single crystals, Adv. Photon. Res. **4**, 2300017 (2023).

[10] H. Yin, Y. Xian, Y. Zhang, W. Chen, X. Wen, N. U. Rahman, Y. Long, B. Jia, J. Fan, and W. Li, An emerging lead-free double-perovskite $Cs_2AgFeCl_6$: In single crystal, Adv. Funct. Mater. **30**, 2002225 (2020).

[11] F. Ji, Ph.D. thesis, Linköping University, 2021.

[12] P. Han, C. Luo, W. Zhou, J. Hou, C. Li, D. Zheng, and K. Han, Band-gap engineering of lead-free iron-based halide double-perovskite single crystals and nanocrystals by an alloying or doping strategy, J. Phys. Chem. C **125**, 11743 (2021).

[13] H.-J. Koo, D. Dai, and M.-H. Whangbo, Importance of supersuperexchange interactions in determining the dimensionality of magnetic properties. determination of strongly interacting spin exchange paths in $A_2Cu(PO_4)_2$ (A = Ba, Sr), $ACuP_2O_7$ (Ba, Ca, Sr, Pb), $CaCuGe_2O_6$, and $Cu_2UO_2(PO_4)_2$ on the basis of qualitative spin dimer analysis, Inorg. Chem. **44**, 4359 (2005).

[14] X. Zhang, K. Liu, J.-Q. He, H. Wu, Q.-Z. Huang, J.-H. Lin, Z.-Y. Lu, and F.-Q. Huang, Antiperovskite chalco-halides $Ba_3(FeS_4)Cl$, $Ba_3(FeS_4)Br$, and $Ba_3(FeSe_4)Br$ with spin super-super exchange, Sci. Rep. **5**, 15910 (2015).

[15] S. Curtarolo, W. Setyawan, G. L. Hart, M. Jahnatek, R. V. Chepulskii, R. H. Taylor, S. Wang, J. Xue, K. Yang, O. Levy, M. J. Mehl, H. T. Stokes, D. O. Demchenko, and D. Morgan, Aflow: An automatic framework for high-throughput materials discovery, Comput. Mater. Sci. **58**, 218 (2012).

[16] A. Jain, S. P. Ong, G. Hautier, W. Chen, W. D. Richards, S. Dacek, S. Cholia, D. Gunter, D. Skinner, G. Ceder, and K. A. Persson, Commentary: The materials project: A materials genome approach to accelerating materials innovation, APL Mater. **1**, 011002 (2013).

[17] Y. Cai, W. Xie, Y. T. Teng, P. C. Harikesh, B. Ghosh, P. Huck, K. A. Persson, N. Mathews, S. G. Mhaisalkar, M. Sherburne, and M. Asta, High-throughput computational study of halide double perovskite inorganic compounds, Chem. Mater. **31**, 5392 (2019).

[18] C. J. Bartel, J. M. Clary, C. Sutton, D. Vigil-Fowler, B. R. Goldsmith, A. M. Holder, and C. B. Musgrave, Inorganic halide double perovskites with optoelectronic properties modulated by sublattice mixing, J. Am. Chem. Soc. **142**, 5135 (2020).

[19] See Supplemental Material at http://link.aps.org/supplemental/10.1103/PhysRevMaterials.7.114404 for the following. Table S1: structural, electronic, and magnetic properties of candidate halide double perovskites considered in this study; Fig. S1: density of states for various $Cs_2BB'Cl_6$ perovskites; Fig. S2: variation of in-plane J_i with U_{eff} for $Cs_2AgNiCl_6$ and $Cs_2NaFeCl_6$; Fig. S3: phonon dispersion at T = 0 K for $Cs_2AgNiCl_6$ (I4/mmm), $Cs_2AuNiCl_6$ (I4/mmm), and $Cs_2HgCrCl_6$ (Fm$\bar{3}$m).

[20] C. J. Bartel, C. Sutton, B. R. Goldsmith, R. Ouyang, C. B. Musgrave, L. M. Ghiringhelli, and M. Scheffler, New tolerance factor to predict the stability of perovskite oxides and halides, Sci. Adv. **5**, eaav0693 (2019).

[21] H. J. Xiang, E. J. Kan, S.-H. Wei, M.-H. Whangbo, and X. G. Gong, Predicting the spin-lattice order of frustrated systems from first principles, Phys. Rev. B **84**, 224429 (2011).

[22] N. S. Fedorova, A. Bortis, C. Findler, and N. A. Spaldin, Four-spin ring interaction as a source of unconventional magnetic orders in orthorhombic perovskite manganites, Phys. Rev. B **98**, 235113 (2018).

[23] G. Kresse and J. Furthmüller, Efficiency of *ab-initio* total energy calculations for metals and semiconductors using a plane-wave basis set, Comput. Mater. Sci. **6**, 15 (1996).

[24] G. Kresse and J. Furthmüller, Efficient iterative schemes for ab initio total-energy calculations using a plane-wave basis set, Phys. Rev. B **54**, 11169 (1996).

[25] G. Kresse and D. Joubert, From ultrasoft pseudopotentials to the projector augmented-wave method, Phys. Rev. B **59**, 1758 (1999).

[26] P. E. Blöchl, Projector augmented-wave method, Phys. Rev. B **50**, 17953 (1994).

[27] Available PAW potentials, https://www.vasp.at/wiki/index.php/Available_PAW_potentials.

[28] J. P. Perdew, A. Ruzsinszky, G. I. Csonka, O. A. Vydrov, G. E. Scuseria, L. A. Constantin, X. Zhou, and K. Burke, Restoring the density-gradient expansion for exchange in solids and surfaces, Phys. Rev. Lett. **100**, 136406 (2008).

[29] S. L. Dudarev, G. A. Botton, S. Y. Savrasov, C. J. Humphreys, and A. P. Sutton, Electron-energy-loss spectra and the structural stability of nickel oxide: An LSDA+U study, Phys. Rev. B **57**, 1505 (1998).

[30] J. Klarbring, U. Singh, S. I. Simak, and I. A. Abrikosov, Electronic structure of the magnetic halide double perovskites Cs_2(Ag, Na)$FeCl_6$ from first principles, Phys. Rev. Mater. **7**, 044605 (2023).

[31] B. Skubic, J. Hellsvik, L. Nordström, and O. Eriksson, A method for atomistic spin dynamics simulations: Implementation and examples, J. Phys.: Condens. Matter **20**, 315203 (2008).

[32] K. Binder, Finite size scaling analysis of ising model block distribution functions, Z. Phys. B **43**, 119 (1981).

[33] K. Binder, Critical properties from Monte Carlo coarse graining and renormalization, Phys. Rev. Lett. **47**, 693 (1981).

[34] D. P. Landau and K. Binder, *A Guide to Monte Carlo Simulations in Statistical Physics*, 3rd ed. (Cambridge University Press, Cambridge, UK, 2009).

[35] R. Dronskowski and P. E. Bloechl, Crystal orbital Hamilton populations (COHP): Energy-resolved visualization of chemical bonding in solids based on density-functional calculations, J. Phys. Chem. **97**, 8617 (1993).

[36] V. L. Deringer, A. L. Tchougréeff, and R. Dronskowski, Crystal orbital Hamilton population (COHP) analysis as projected from plane-wave basis sets, J. Phys. Chem. A **115**, 5461 (2011).

[37] S. Maintz, V. L. Deringer, A. L. Tchougréeff, and R. Dronskowski, Analytic projection from plane-wave and PAW wavefunctions and application to chemical-bonding analysis in solids, J. Comput. Chem. **34**, 2557 (2013).

[38] R. Nelson, C. Ertural, J. George, V. L. Deringer, G. Hautier, and R. Dronskowski, LOBSTER: Local orbital projections, atomic charges, and chemical-bonding analysis from projector-augmented-wave-based density-functional theory, J. Comput. Chem. **41**, 1931 (2020).

[39] A. Togo, First-principles phonon calculations with phonopy and phono3py, J. Phys. Soc. Jpn. **92**, 012001 (2023).

[40] A. Togo, L. Chaput, T. Tadano, and I. Tanaka, Implementation strategies in phonopy and phono3py, J. Phys.: Condens. Matter **35**, 353001 (2023).

[41] R. A. de Groot, F. M. Mueller, P. G. vanEngen, and K. H. J. Buschow, New class of materials: Half-metallic ferromagnets, Phys. Rev. Lett. **50**, 2024 (1983).

[42] M. I. Katsnelson, V. Y. Irkhin, L. Chioncel, A. I. Lichtenstein, and R. A. de Groot, Half-metallic ferromagnets: From band structure to many-body effects, Rev. Mod. Phys. **80**, 315 (2008).

[43] I. Žutić, J. Fabian, and S. Das Sarma, Spintronics: Fundamentals and applications, Rev. Mod. Phys. **76**, 323 (2004).

[44] M. Jourdan, J. Minár, J. Braun, A. Kronenberg, S. Chadov, B. Balke, A. Gloskovskii, M. Kolbe, H. J. Elmers, G. Schönhense, H. Ebert, C. Felser, and M. Kläui, Direct observation of half-metallicity in the Heusler compound Co_2MnSi, Nat. Commun. **5**, 3974 (2014).

[45] A. Kundu, S. Ghosh, R. Banerjee, S. Ghosh, and B. Sanyal, New quaternary half-metallic ferromagnets with large curie temperatures, Sci. Rep. **7**, 1803 (2017).

[46] D. M. Korotin, V. V. Mazurenko, V. I. Anisimov, and S. V. Streltsov, Calculation of exchange constants of the Heisenberg model in plane-wave-based methods using the Green's function approach, Phys. Rev. B **91**, 224405 (2015).

[47] A. E. Maughan, A. M. Ganose, M. M. Bordelon, E. M. Miller, D. O. Scanlon, and J. R. Neilson, Defect tolerance to

intolerance in the vacancy-ordered double perovskite semiconductors Cs_2SnI_6 and Cs_2TeI_6, J. Am. Chem. Soc. **138**, 8453 (2016).

[48] A. E. Maughan, A. M. Ganose, A. M. Candia, J. T. Granger, D. O. Scanlon, and J. R. Neilson, Anharmonicity and octahedral tilting in hybrid vacancy-ordered double perovskites, Chem. Mater. **30**, 472 (2018).

[49] A. E. Maughan, A. M. Ganose, D. O. Scanlon, and J. R. Neilson, Perspectives and design principles of vacancy-ordered double perovskite halide semiconductors, Chem. Mater. **31**, 1184 (2019).

[50] U.-G. Jong, C.-J. Yu, Y.-H. Kye, S.-H. Choe, J.-S. Kim, and Y.-G. Choe, Anharmonic phonons and phase transitions in the vacancy-ordered double perovskite Cs_2SnI_6 from first-principles predictions, Phys. Rev. B **99**, 184105 (2019).

[51] S. R. Kavanagh, C. N. Savory, S. M. Liga, G. Konstantatos, A. Walsh, and D. O. Scanlon, Frenkel excitons in vacancy-ordered titanium halide perovskites (Cs_2TiX_6), J. Phys. Chem. Lett. **13**, 10965 (2022).

[52] G. Ji, C. Han, S. Hu, P. Fu, X. Chen, J. Guo, J. Tang, and Z. Xiao, B-site columnar-ordered halide double perovskites: Theoretical design and experimental verification, J. Am. Chem. Soc. **143**, 10275 (2021).

[53] Z. Fang, K. Terakura, and J. Kanamori, Strong ferromagnetism and weak antiferromagnetism in double perovskites: Sr_2FeMO_6, M = Mo, W, and Re, Phys. Rev. B **63**, 180407(R) (2001).

[54] K.-I. Kobayashi, T. Kimura, H. Sawada, K. Terakura, and Y. Tokura, Room-temperature magnetoresistance in an oxide material with an ordered double-perovskite structure, Nature (London) **395**, 677 (1998).

[55] A. Sleight and J. Weiher, Magnetic and electrical properties of Ba_2MReO_6 ordered perovskites, J. Phys. Chem. Solids **33**, 679 (1972).

[56] H. Kawanaka, I. Hase, S. Toyama, and Y. Nishihara, Electronic state of fe in double perovskite oxide Sr_2FeWO_6, J. Phys. Soc. Jpn. **68**, 2890 (1999).

[57] A. Karmakar, M. S. Dodd, S. Agnihotri, E. Ravera, and V. K. Michaelis, Cu(II)-doped $Cs_2SbAgCl_6$ double perovskite: A lead-free, low-bandgap material, Chem. Mater. **30**, 8280 (2018).

[58] X. Wang, J. Yang, X. Wang, M. Faizan, H. Zou, K. Zhou, B. Xing, Y. Fu, and L. Zhang, Entropy-driven stabilization of multielement halide double-perovskite alloys, J. Phys. Chem. Lett. **13**, 5017 (2022).

[59] W. Ning, J. Bao, Y. Puttisong, F. Moro, L. Kobera, S. Shimono, L. Wang, F. Ji, M. Cuartero, S. Kawaguchi, S. Abbrent, H. Ishibashi, R. D. Marco, I. A. Bouianova, G. A. Crespo, Y. Kubota, J. Brus, D. Y. Chung, L. Sun, W. M. Chen *et al.*, Magnetizing lead-free halide double perovskites, Sci. Adv. **6**, eabb5381 (2020).

[60] P. Debye, Einige bemerkungen zur magnetisierung bei tiefer temperatur, Ann. Phys. (Leipzig) **386**, 1154 (1926).

[61] W. F. Giauque, A thermodynamic treatment of certain magnetic effects. a proposed method of producing temperatures considerably below 1° absolute, J. Am. Chem. Soc. **49**, 1864 (1927).

[62] W. F. Giauque and D. P. MacDougall, Attainment of temperatures below 1° absolute by demagnetization of $Gd_2(SO_4)_3.8H_2O$, Phys. Rev. **43**, 768 (1933).

[63] A. Boutahar, R. Moubah, E. K. Hlil, H. Lassri, and E. Lorenzo, Large reversible magnetocaloric effect in antiferromagnetic Ho_2O_3 powders, Sci. Rep. **7**, 13904 (2017).

[64] L. C. Wang, Q. Y. Dong, Z. Y. Xu, F. X. Hu, J. R. Sun, and B. G. Shen, Low-temperature large magnetocaloric effect in the antiferromagnetic $ErNi_{0.6}Cu_{0.4}Al$ compound, J. Appl. Phys. **113**, 023916 (2013).

[65] X. Tan, P. Chai, C. M. Thompson, and M. Shatruk, Magnetocaloric effect in $AlFe_2B_2$: Toward magnetic refrigerants from earth-abundant elements, J. Am. Chem. Soc. **135**, 9553 (2013).

[66] O. Tegus, E. Brück, K. H. J. Buschow, and F. R. de Boer, Transition-metal-based magnetic refrigerants for room-temperature applications, Nature (London) **415**, 150 (2002).

[67] T. Krenke, E. Duman, M. Acet, E. F. Wassermann, X. Moya, L. Mañosa, and A. Planes, Inverse magnetocaloric effect in ferromagnetic $Ni - Mn - Sn$ alloys, Nat. Mater. **4**, 450 (2005).

[68] T. Katase, Y. Suzuki, and H. Ohta, Reversibly switchable electromagnetic device with leakage-free electrolyte, Adv. Electron. Mater. **2**, 1600044 (2016).

[69] H. Wu, H. Zhang, B. Wang, F. Groß, C.-Y. Yang, G. Li, C. Guo, H. He, K. Wong, D. Wu, X. Han, C.-H. Lai, J. Gräfe, R. Cheng, and K. L. Wang, Current-induced néel order switching facilitated by magnetic phase transition, Nat. Commun. **13**, 1629 (2022).